Kovove Mater. 62 2024 21–30
DOI: 10.31577/km.2024.1.21

The effect of deformation temperature in metastable austenite zone on microstructure evolution, mechanical and corrosion properties of high Cr ferritic-martensitic steel

Wanjun Wang[1], Xuan Wang[1], Yinghui Lv[1], Yingkun Wu[1], Jianguo Chen[2]*

[1] *Tianjin Special Equipment Inspection Institute, Tianjin 300192, P. R. China*
[2] *School of Mechanical Engineering, Tianjin Sino-German University of Applied Sciences, Tianjin 300350, P. R. China*

Received 11 May 2023, received in revised form 7 March 2024, accepted 7 March 2024

Abstract

This work investigated the impact of deformation temperature in metastable austenite zone on microstructure evolution and mechanical and corrosion properties of high Cr ferritic-martensitic steel. The martensitic lath characteristics and the size and distribution of precipitates of the steels were observed using transmission electron microscopy (TEM). The results show that narrowing of the lath width occurs as the deformation temperature reduces from 800 to 600 °C. During subsequent high-temperature tempering, the martensitic lath recovery degree of the tempered steel gradually increases, and the size of the precipitates gradually decreases with the decrease of the previous deformation temperature. A tensile test was conducted on the steels subjected to high-temperature tempering. The tensile strength of deformed steel is found to be higher than that of undeformed steel. The tensile properties of the deformed steels decrease with the decrease of the deformation temperature. The electrochemical polarization curve confirms that the corrosion resistance of the deformed steel subjected to tempering is gradually improved with decreasing deformation temperature. This work clarifies the influence mechanism of deformation temperature on the microstructure and properties of high Cr ferritic-martensitic steel and provides a reliable basis for actual industrial production.

K e y w o r d s: deformation temperature, high-temperature tempering, microstructure, mechanical property, corrosion resistance

1. Introduction

High Cr ferritic-martensitic steels are widely utilized in high-temperature components such as main steam and superheater piping of advanced thermal power plants due to their low thermal expansion coefficient, exceptional high-temperature mechanical properties, and cost-effectiveness [1–5]. Typically, they are put into service after being rolled into tubes and subjected to high-temperature tempering treatment, because high-temperature tempering can enhance the mechanical performance by improving the precipitation strengthening of steel [6–9]. The microstructure of high-temperature tempered steel is characterized by abundant carbides along the boundaries of tempered martensitic laths and a limited amount of carbides inside the martensitic laths [10–17].

Two practical methods to enhance the properties of high Cr ferritic-martensitic steels are composition optimization and heat treatment design. Although simple composition optimization can improve the strength of the steel, it inevitably leads to the deterioration of the weldability and toughness [18–20]. Therefore, microstructure control and precipitation reinforcement caused by the special heat treatment process design is an effective method to improve the properties of steel. Deformation heat treatment has been widely studied as a commonly used special heat treatment method. Until now, some studies have been carried out on improving the microstructure and mechanical properties of high Cr ferritic-martensitic steel by deformation heat treatment [21, 22]. Tan et al. [23] found that the strength and hardness of steel at room temperature significantly in-

*Corresponding author: e-mail address: jianguo_chen123@163.com

creased as the deformation degree increased from 25 to 45 %, especially, the maximum hardness increased by 29 % and the yield strength increased by 47 % during deformation heat treatment compared to the steel in the traditional normalizing and tempering condition. Zhou et al. [5] reported that the martensitic lath can be significantly refined by applying compressive stress during the formation of martensite formation, thus improving the high-temperature mechanical properties of the steel, which is specifically reflected in the increase of the yield strength from 339 to 378 MPa at 600 ℃. Zhang et al. [24] confirmed that dynamic plastic deformation can effectively refine the microstructure of steel. As the strain increases from 0.5 to 2.3, the lath boundary spacing decreases from 190 nm to 98 nm, and the ultimate tensile strength increases from 675 to 1247 MPa. However, current investigations focus on the effect of deformation degree on the microstructure and mechanical properties of high Cr ferritic-martensitic steel, while the research on deformation temperature, another important parameter in the deformation heat treatment process of actual production, is very limited. Additionally, most research focuses solely on mechanical properties, neglecting the importance of evaluating corrosion resistance in practical applications [25].

This study comprehensively investigates the impact of deformation temperature in the metastable austenite zone on the microstructure evolution, mechanical property and corrosion resistance of high Cr ferritic-martensitic steel by transmission electron microscopy (TEM), tensile testing, and electrochemical polarization curve analysis. The mechanism of microstructural evolution and its effect on mechanical and corrosion properties were discussed in detail.

2. Materials and experimental methods

2.1. Samples preparation

A vacuum induction furnace produced a 28 kg ingot that was further forged into a cylindrical bar measuring 350 mm in height and 120 mm in diameter. Table 1 lists the chemical composition of the steel. Figure 1 shows the original microstructure composed of martensite, as captured using an optical microscope (OM, Leica DMI 5000m). It is worth noting that Fig. 1 is also presented in [26], as both works share the same sample batch.

Samples were cut from the middle section of the steel bar using wire-electrode cutting to conduct the rolling deformation test. These samples were subsequently heated to 1050 ℃ at a rate of 200 ℃ min^{-1} and maintained for 30 minutes. Afterwards, they were cooled to 800, 700, and 600 ℃ at a cooling rate of 200 ℃ min^{-1} and rolled to a 40 % reduction in height before air cooling. All the deformed samples were subjected to a high-temperature tempering treatment at 750 ℃ for 90 minutes. Figure 2 illustrates the specific heat treatment process flow.

Table 1. Chemical composition of the steel (wt.%)

C	Cr	W	Mn	Si	V	Ta	Fe
0.04	8.93	1.72	0.44	0.04	0.22	0.07	Bal.

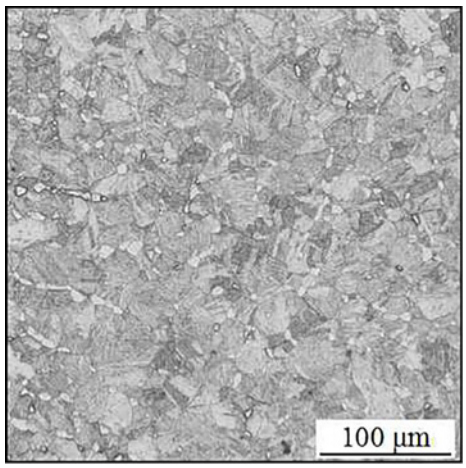

Fig. 1. OM image of the original microstructure of the high Cr ferritic-martensitic steel.

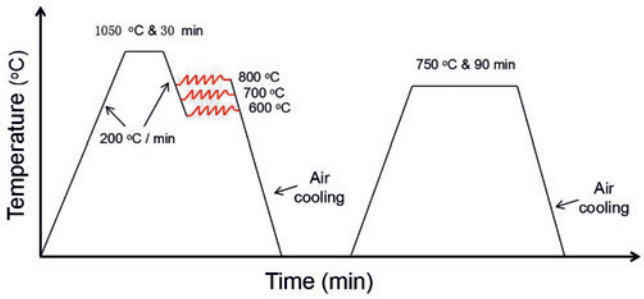

Fig. 2. Flow diagram of deformation and high-temperature tempering treatment of the high Cr ferritic-martensitic steel.

2.2. Microstructure observation

The characteristics of martensitic lath in the deformed high Cr ferritic-martensitic steels and the size and distribution of martensitic lath and the second phase after subsequent high-temperature tempering were observed by Jem-2100f transmission electron microscope (TEM). Metal thinning samples were used to

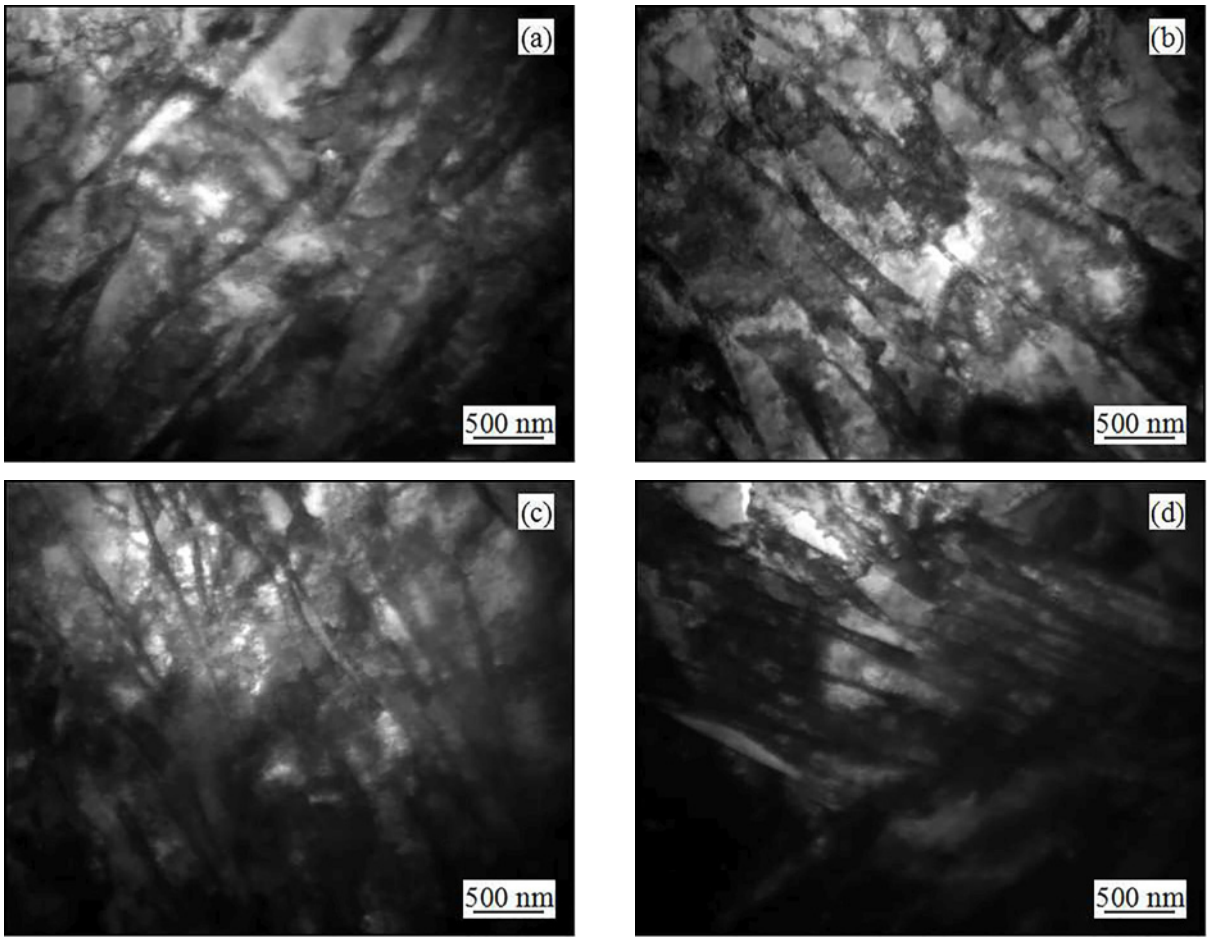

Fig. 3. TEM images of metal thinning samples of the high Cr ferritic-martensitic steels deformed at different temperatures: (a) directly cooling without deformation, (b) 800 °C, (c) 700 °C, and (d) 600 °C.

observe the martensitic laths. Thin slices with a thickness of 0.3 mm were cut from the samples and manually ground to about 50 μm. Small discs 3 mm in diameter were made using a punch and then thinned on an MTP-1A magnetic-driven double-spray electrolytic thinning machine. The electrolytic double spray solution is a mixture of 5 % perchloric acid and 95 % alcohol. An electrolytic voltage of 40 V and a temperature of −20 °C were employed. Since the second phase of the steel is obscured by the diffraction contrast in the metal foil, the carbon extraction replica technique was used to observe the size and distribution of the second phase of the steel [27]. After deep etching and carbon coating on the surface of polished samples, the surface was lightly carved into a square with a side length of about 2 mm and then soaked in a mixed solution of 30 mL hydrochloric acid, 30 mL alcohol and 5 g $CuCl_2$ until the carbon film fell off. The detached carbon films were finished using small copper mesh and washed with alcohol and water before finally being dried on filter paper.

2.3. Mechanical test

To evaluate the mechanical properties of high Cr ferritic-martensitic steels with different deformation temperatures subjected to subsequent high-temperature tempering, tensile tests were conducted using an Instron 8871 machine. Tensile samples with a gauge length of 8 mm and a thickness of 2 mm were tested at room temperature using a strain rate of $1.0 \times 10^{-4}\ s^{-1}$. Three samples were tested under each condition for the tensile test.

2.4. Electrochemical test

Electrochemical polarization curves were utilized to measure the corrosion resistance of high Cr ferritic-martensitic steels with different deformation temperatures subjected to subsequent high-temperature tempering. Electrochemical testing is carried out in 3.5 wt.% NaCl solution at room temperature. The polarization curves were generated using a PARSTAT 4000A electrochemical workstation, applying test methods and parameter settings outlined in [28].

3. Results and discussion

3.1. Microstructure of the high Cr ferritic-martensitic steels

3.1.1. TEM observation of the deformed steels

Figure 3 shows the TEM images of metal thinning samples for high Cr ferritic-martensitic steels deformed at varying temperatures. A noticeable observation is that as the deformation temperature decreases, there is a significant increase in the refinement trend of the martensitic laths. Additionally, the width of the laths becomes uneven, and their length becomes shorter while the orientation relationship between the laths becomes inconsistent. The observed changes arise due to the strain defects introduced during the deformation process that enable more martensite nucleation sites, causing greater competition among martensitic laths. As a result, the width of the laths becomes uneven, and their orientation relationship loses its original parallel state.

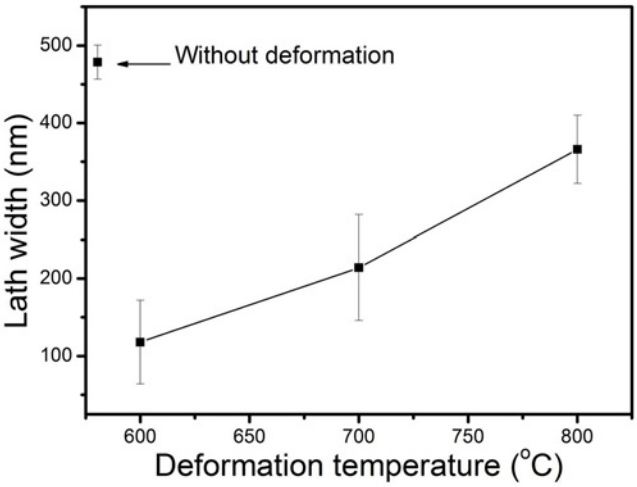

Fig. 4. Martensitic lath width of the high Cr ferritic--martensitic steels deformed at different temperatures.

Figure 4 presents the average width of martensitic lath of high Cr ferritic-martensitic steels deformed at

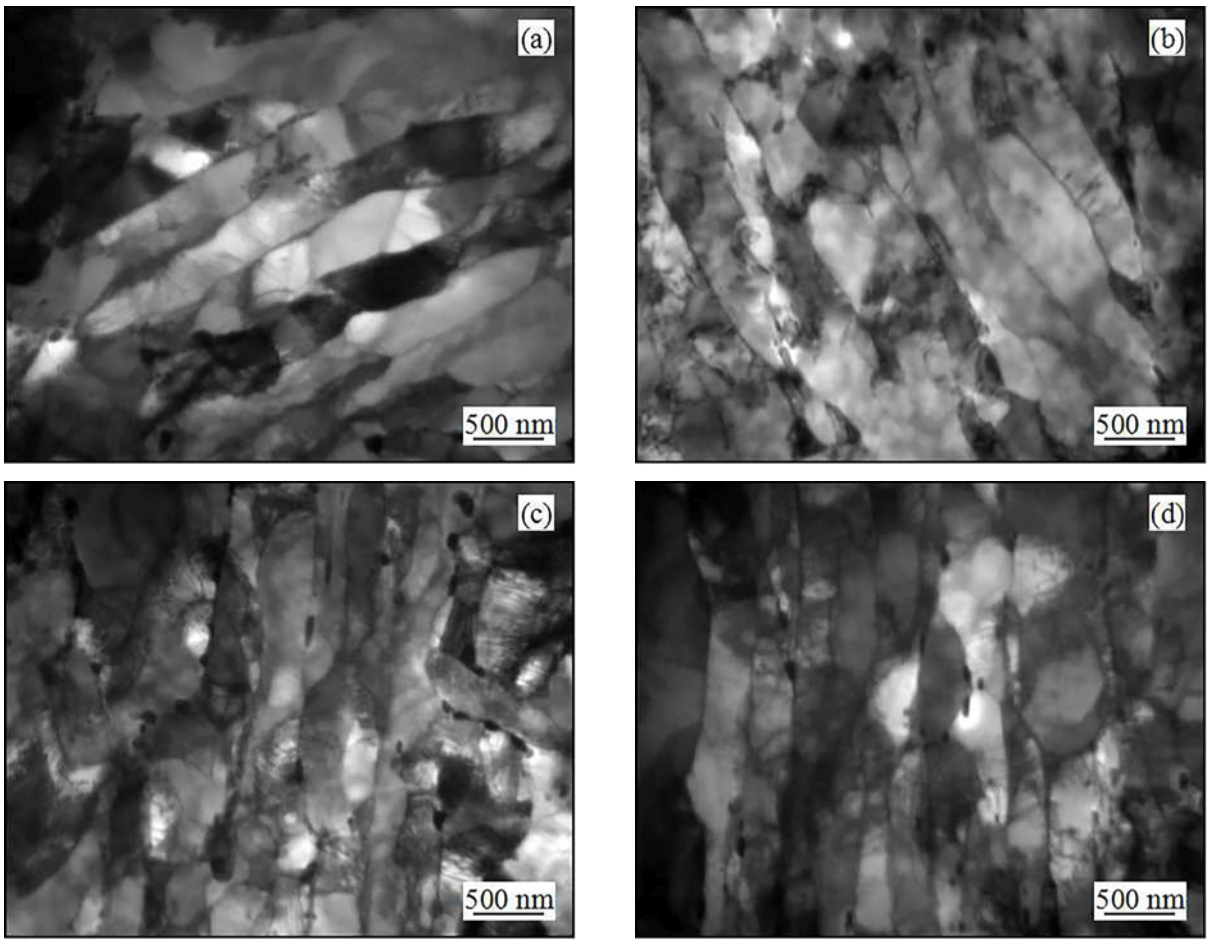

Fig. 5. TEM images of metal thinning samples of the deformed high Cr ferritic-martensitic steels subjected to high-temperature tempering: (a) directly cooling without deformation, (b) 800 ℃, (c) 700 ℃, and (d) 600 ℃.

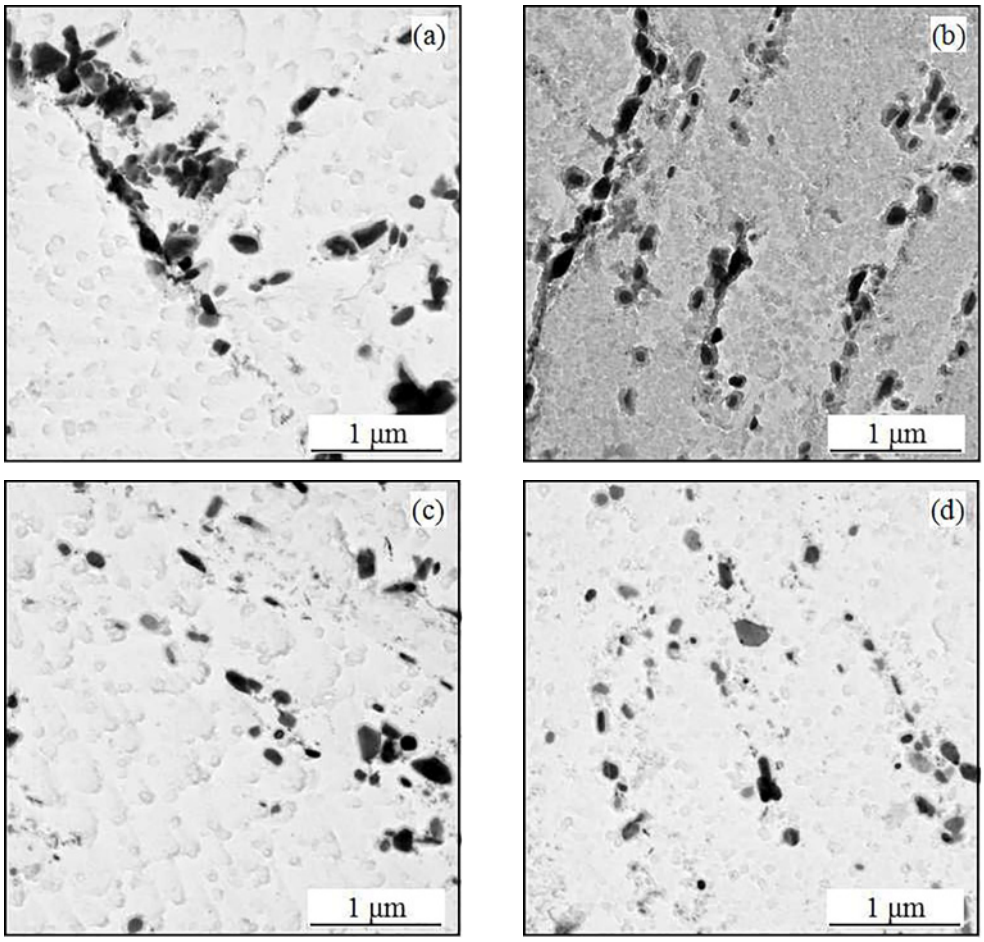

Fig. 6. TEM images of extraction replica samples of the deformed high Cr ferritic-martensitic steels subjected to high--temperature tempering: (a) directly cooling without deformation, (b) 800 ℃, (c) 700 ℃, and (d) 600 ℃.

various temperatures. The martensitic lath width was measured using the intercept method in the direction perpendicular to the lath length, followed by statistical analysis [29]. The statistical outcomes demonstrate that the martensitic lath width of the undeformed steel is the largest. The martensitic lath width for deformed steel reduces from 366 to 118 nm as the deformation temperature decreases from 800 to 600 ℃. The reduction in lath width can be attributed to the lower recovery and recrystallization of the parent phase at lower deformation temperatures, which increases the austenite defect numbers before martensitic transformation, leading to the corresponding increase of martensite nucleation positions and then results in the refinement of martensitic laths [30].

3.1.2. TEM observation of the deformed steels subjected to high-temperature tempering

Figure 5 displays the TEM images of metal thinning samples of the deformed high Cr ferritic-martensitic steels subjected to high-temperature tempering. These samples predominantly exhibit the typical tempered martensitic lath morphology. However, partial recovery of laths was observed in tempered samples with low deformation temperatures. The decrease in deformation temperature from 800 to 600 ℃ results in a gradual blurring of martensitic lath characteristics, accompanied by the appearance of Y-junctions (Y-shaped grain boundaries). This reflects the destruction of the parallel orientation relationship between the laths, signifying that the decrease in deformation temperature accelerates martensitic lath recovery during high-temperature tempering. This can be attributed to decreased apparent recovery activation energy due to lower deformation temperature [30]. Although the local recovery of martensitic lath has occurred, it can be found from the figure that the dislocation density of the deformed samples is higher than that of the undeformed sample. This is because the increase in dislocation density in the microstructure caused by rolling deformation is larger than the decrease caused by the subsequent tempering process, as evidenced in previous research by Mao et al. [31].

Figure 6 shows the TEM images of carbon extraction replica samples of the deformed high Cr ferritic-

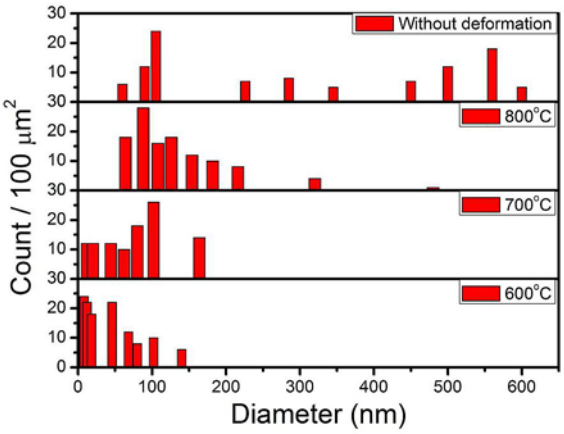

Fig. 7. Density and size of carbide in the tempered high Cr ferritic-martensitic steels after different deformation temperatures.

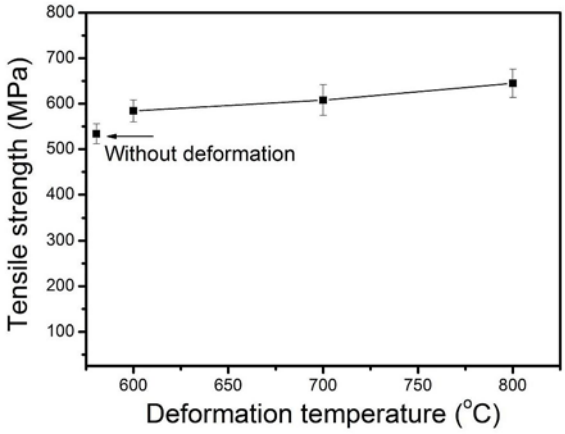

Fig. 8. Tensile property of the deformed high Cr ferritic-martensitic steels subjected to high-temperature tempering.

-martensitic steels subjected to high-temperature tempering. The precipitates are primarily found along the grain boundaries or martensitic lath boundaries due to the high interfacial energy in these regions. Previous studies have confirmed that the precipitates formed in the rolled high Cr ferritic-martensitic steel during high-temperature tempering are Cr-rich carbides [31]. Deformation in the metastable austenite zone results in the fragmentation of the martensitic laths, creating more opportunities for carbide nucleation during subsequent high-temperature tempering. In addition, deformation increases the number of internal defects in martensitic laths, which evolve into subgrain boundaries during tempering, providing a higher level of nucleation sites for carbides [32]. As previously analyzed, lower deformation temperatures result in greater deformation of the martensitic laths, forming more subgrain boundaries for carbide nucleation during tempering. Consequently, the carbide particles exhibit finer distribution.

To quantify the distribution of the Cr-rich carbides in deformed high Cr ferritic-martensitic steels subjected to high-temperature tempering, the size and quantity of carbides were statistically analyzed, and the statistical results are presented in Fig. 7. It can be observed that the carbide in undeformed tempered steel is the largest. As the deformation temperature decreases, the carbides in the deformed steel become finer during the subsequent high-temperature tempering. This observation is consistent with the findings from Fig. 5. It is fully explained that the deformed or fractured martensitic laths and their internal dislocation caused by low deformation temperature have a higher likelihood of recovering or recrystallizing in the subsequent high-temperature tempering, resulting in the formation of more boundaries for carbide nucleation. Since all samples were taken from the same steel bar, the carbon content in all samples is equal. Under the premise of the same carbon content, the increased number of nucleation sites resulted in a finer distribution of carbides.

3.2. Mechanical and corrosion properties of the deformed high Cr ferritic-martensitic steels subjected to high-temperature tempering

3.2.1. Mechanical properties

Figure 8 shows the tensile properties of the deformed high Cr ferritic-martensitic steels subjected to high-temperature tempering. It is evident that the strength of deformed steels after tempering is higher than that of undeformed steel (536 MPa), which is due to the refinement of martensitic lath, the increase of dislocation density and the uniform distribution of precipitates caused by deformation. For deformed steels, the tensile property decreases from 645 to 584 MPa, with the deformation temperature decreasing from 800 to 600 ℃. This can be explained by the low recovery degree of the sample after high-temperature deformation during the subsequent high-temperature tempering process. Moreover, the pinning effect of uniformly distributed precipitates on grain boundaries, lath boundaries and dislocations is enhanced, increasing tensile properties. However, after low-temperature deformation, the martensitic lath recovery degree of the sample in the subsequent tempering is significantly enhanced. Since the recovery of martensitic lath is a process of dislocation movement and annihilation [33], the increase in recovery degree leads to decreased dislocation density. At this time, precipitation strengthening cannot compensate for the strength reduction caused by dislocation annihilation.

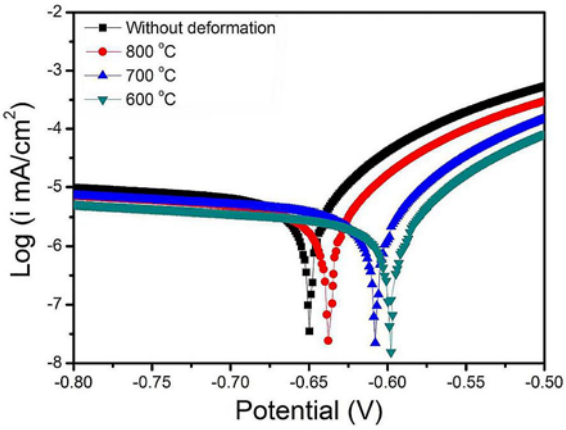

Fig. 9. Electrochemical polarization curves of the deformed high Cr ferritic-martensitic steels subjected to high-temperature tempering in 3.5 wt.% NaCl solution at room temperature.

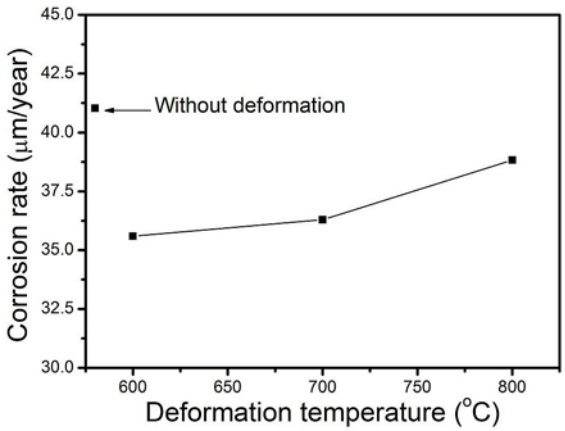

Fig. 10. Corrosion rate of the tempered high Cr ferritic-martensitic steels with different deformation temperatures.

Table 2. Electrochemical parameters of the deformed high Cr ferritic-martensitic steels after high-temperature tempering in 3.5 wt.% NaCl solution at room temperature

Deformation temperature (℃)	E_{corr} (V)	i_{corr} (μA cm^{-2})
Without deformation	–0.649	3.55
800	–0.638	3.36
700	–0.607	3.14
600	–0.598	3.08

3.2.2. Corrosion properties

Figure 9 shows the electrochemical polarization curves of the deformed high Cr ferritic-martensitic steels subjected to high-temperature tempering in 3.5 wt.% NaCl solution at room temperature. The polarization curves of all samples exhibit similar shapes and trends. Corrosion potential (E_{corr}) and corrosion current density (i_{corr}) were analyzed as the main parameters for evaluating corrosion performance. E_{corr} was directly read from the polarization curve, while i_{corr} was calculated through Tafel extrapolation of the anodic and cathodic branches [34]. Table 2 presents the E_{corr} and i_{corr} of all samples. It can be seen that the undeformed tempered steel has the maximum i_{corr} and the minimum E_{corr}. For deformed steel, the i_{corr} of the sample after subsequent high-temperature tempering decreases as the deformation temperature decreases, while the E_{corr} shows an upward trend.

Corrosion rate (C_r, expressed in μm year^{-1}) is a crucial metric used to determine the corrosion resistance of materials, which can be calculated using the following formula [35]:

$$C_r = (3.27 \times i_{corr} \times A)/nD, \quad (1)$$

where A is the atomic weight, n is the number of electrons exchanged in the electrochemical reaction, and D is the material density. Considering that the samples in this work are iron-based metal samples, A is 55.84, D is 7.90 g cm^{-3}, and n is 2 [36]. Figure 10 shows the calculated corrosion rate of the tempered high Cr ferritic-martensitic steels with different deformation temperatures. The results indicate that the highest corrosion rate is observed in the undeformed tempered steel, with a value of 41.03. For deformed steel, as the deformation temperature decreases from 800 to 600 ℃, the corrosion rate decreases from 38.83 to 35.59.

The enhanced corrosion resistance of the high Cr ferritic-martensitic steels deformed in the metastable austenite region subjected to high-temperature tempering is associated with the evolution of Cr-rich carbides within the matrix. A previous study has confirmed that a phase potential difference between the Cr-rich carbides and the matrix can create local galvanic couples, which may decrease corrosion resistance [37]. Uneven distribution of Cr-rich carbide size can lead to the formation of local galvanic couples, resulting in weaker corrosion resistance [38]. For the undeformed tempered steel, the size of the Cr-rich carbides precipitated at the prior austenite grain boundaries and the martensitic lath boundaries is larger, and the concentration of Cr element in the large-sized carbides is greater than that in the surrounding areas, resulting in the formation of local Cr-depleted zones, which increases the likelihood of corrosion occurrence at these locations [39–41]. Meanwhile, large-sized carbides have low pitting potential and decrease the corrosion resistance of steel [42]. Conversely, for deformed steel, as the deformation temperature decreases, more subgrain boundaries for carbide nucleation are formed in the subsequent tempering process. This results in

smaller and more evenly distributed Cr-rich carbides, reducing the possibility of forming local galvanic couples and/or local Cr concentration differences [43, 44]. As a result, the corrosion resistance of steel is improved.

4. Conclusions

This study investigated the impact of deformation temperature in metastable austenite zone on the microstructure and mechanical and corrosion properties of high Cr ferritic-martensitic steel. The main findings are as follows:

(1) The deformation refines the martensitic lath width of the steel. As the deformation temperature decreases from 800 to 600 ℃, the average width of the martensitic lath decreases from 366 to 118 nm. After deformation at 600 ℃, the martensitic lath width is extremely uneven, and the orientation between the laths becomes non-parallel.

(2) Lower deformation temperatures result in more significant recovery and recrystallization of the laths and the smaller and denser precipitation of carbides in the deformed steel during the subsequent high-temperature tempering.

(3) The tensile property of the deformed steel subjected to high-temperature tempering decreases with the decrease of the deformation temperature. Compared with the undeformed steel, the deformed steels exhibit higher tensile properties.

(4) Decreasing the deformation temperature decreases the corrosion current density of the deformed steel subjected to high-temperature tempering while simultaneously increasing the corrosion potential. The corrosion rate follows the same trend as that of corrosion current density.

Acknowledgements

The work was financially supported by the Science&Technology Development Fund of Tianjin Education Commission for Higher Education (No. 2023KJ250).

References

[1] J. G. Chen, Y. C. Liu, Y. T. Xiao, Y. H. Liu, C. X. Liu, H. J. Li, Improvement of high-temperature mechanical properties of low-carbon RAFM steel by MX precipitates, Acta Metallurgica Sinica (English Letters) 31 (2018) 706–712. https://doi.org/10.1007/s40195-018-0703-y

[2] V. Sklenička, K. Kuchařová, M. Svoboda, Creep behaviour and microstructure evolution of advanced creep-resistant 9%Cr martensitic steels under cyclic thermal loading, Kovove Materialy-Metallic Materials 56 (2018) 1–13. https://doi.org/10.4149/km_2018_1_1

[3] J. G. Chen, Y. C. Liu, C. X. Liu, B. Y. Yan, H. J. Li, Effects of tantalum on austenitic transformation kinetics of RAFM steel, Journal of Iron and Steel Research International 24 (2017) 705–710. https://doi.org/10.1016/s1006-706x(17)30106-1

[4] C. Wei, H. W. Zhang, Z. J. Wang, Y. S. Wei, J. G. Chen, Adverse effects of continuous oxides at the diffusion bonding interface of RAFM steels and the improvement of joint strength by bonding pressure, Materials Today Communications 31 (2022) 103840. https://doi.org/10.1016/j.mtcomm.2022.103840

[5] X. S. Zhou, C. X. Liu, L. M. Yu, Y. C. Liu, H. J. Li, Phase transformation behavior and microstructural control of high Cr martensitic/ferritic heat-resistant steels for power and nuclear plants: A review, Journal of Materials Science & Technology 31 (2015) 235–242. https://doi.org/10.1016/j.jmst.2014.12.001

[6] J. W. Zhang, L. M. Yu, Q. Z. Gao, C. X. Liu, Z. Q. Ma, H. J. Li, Y. C. Liu, H. Wang, A new strategy to improve the creep strength of a novel G115 steel by accelerating the precipitation of nano-sized MX and Cu-rich particles, Scripta Materialia 220 (2022) 114903. https://doi.org/10.1016/j.scriptamat.2022.114903

[7] J. W. Zhang, L. M. Yu, Q. Z. Gao, C. X. Liu, Z. Q. Ma, H. J. Li, Y. C. Liu, H. Wang, Creep behavior, microstructure evolution and fracture mechanism of a novel martensite heat resistance steel G115 affected by prior cold deformation, Materials Science and Engineering A 850 (2022) 143564. https://doi.org/10.1016/j.msea.2022.143564

[8] H. S. He, L. M. Yu, C. X. Liu, H. J. Li, Q. Z. Gao, Y. C. Liu, Research progress of a novel martensitic heat-resistant steel G115, Acta Metallurgica Sinica 58 (2022) 311–323. https://doi.org/10.11900/0412.1961.2021.00185

[9] J. G. Chen, C. X. Liu, C. Wei, Y. C. Liu, H. J. Li, Effects of isothermal aging on microstructure and mechanical property of low-carbon RAFM steel, Acta Metallurgica Sinica (English Letters) 32 (2019) 1151–1160. https://doi.org/10.1007/s40195-019-00883-6

[10] X. S. Zhou, G. D. Liu, X. Q. Shen, Y. C. Liu, Tensile strength improvement of martensitic ODS steels with Zr and Hf additions, Materials Science and Engineering A 829 (2022) 142071. https://doi.org/10.1016/j.msea.2021.142071

[11] Z. X. Xia, C. Zhang, H. Lan, Z. G. Yang, TaC precipitation behaviors in reduced activation martensitic steels, Journal of Materials Science 46 (2011) 3151–3156. https://doi.org/10.1007/s10853-010-5196-7

[12] J. G. Chen, C. X. Liu, Y. C. Liu, B. Y. Yan, H. J. Li, Effects of tantalum content on the microstructure and mechanical properties of low-carbon RAFM steel, Journal of Nuclear Materials 479 (2016) 295–301. https://doi.org/10.1016/j.jnucmat.2016.07.029

[13] C. X. Liu, C. L. Mao, L. Cui, X. S. Zhou, L. M. Yu, Y. C Liu, Recent progress in microstructural control and solid-state welding of reduced activation ferritic/martensitic steels, Acta Metallurgica Sinica 57 (2021) 1521–1538. https://doi.org/10.11900/0412.1961.2021.00348

[14] J. G. Chen, Y. C. Liu, C. X. Liu, X. S. Zhou, H. J. Li, Study on microstructural evolution and constitutive modeling for hot deformation behavior of a low-carbon RAFM steel, Journal of Materials Research 32 (2017) 1376–1385. https://doi.org/10.1557/jmr.2017.77

[15] X. S. Zhou, H. K. Dong, Y. S. Wang, M. N. Yuan, Microstructure characteristics and mechanical performance of Fe-Cr-Ni-Al-Ti superalloy fabricated by powder metallurgy, Journal of Alloys and Compounds 918 (2022) 165612. https://doi.org/10.1016/j.jallcom.2022.165612

[16] Z. X. Xia, C. Zhang, Q. Y. Huang, S. J. Liu, Z. D. Li, Z. G. Yang, Effect of TaC particles dissolution on grain coarsening in reduced activation steels, Journal of Iron and Steel Research International 18 (2011) 47–52. https://doi.org/10.1016/S1006-706X(12)60033-8

[17] J. Dong, X. S. Zhou, Y. C. Liu, C. Li, C. X. Liu, Q. Y. Guo, Carbide precipitation in Nb-V-Ti microalloyed ultra-high strength steel during tempering, Materials Science and Engineering A 683 (2017) 215–226. https://doi.org/10.1016/j.msea.2016.12.019

[18] L. Korcakova, J. Hald, M. A. J. Somers, Quantification of Laves phase particle size in 9CrW steel, Materials Characterization 47 (2001) 111–117. https://doi.org/10.1016/S1044-5803(01)00159-0

[19] S. Holmström, P. Auerkari, Predicting weld creep strength reduction for 9 % Cr steels, International Journal of Pressure Vessels and Piping 83 (2006) 803–808. https://doi.org/10.1016/j.ijpvp.2006.08.007

[20] J. A. Francis, W. Mazur, H. K. D. H. Bhadeshia, Type IV cracking in ferritic power plant steels, Materials Science and Technology 22 (2006) 1387–1395. https://doi.org/10.1179/174328406X148778

[21] S. Hollner, E. Piozin, P. Mayr, C. Caës, I. Tournié, A. Pineau, B. Fournier, Characterization of a boron alloyed 9Cr3W3CoVNbBN steel and further improvement of its high-temperature mechanical properties by thermomechanical treatments, Journal of Nuclear Materials 441 (2013) 15–23. https://doi.org/10.1016/j.jnucmat.2013.05.018

[23] J. W. Zhang, L. M. Yu, Q. Z. Gao, C. X. Liu, Z. Q. Ma, H. J. Li, Y. C. Liu, H. Wang, Tailoring the tempered microstructure of a novel martensitic heat resistant steel G115 through prior cold deformation and its effect on mechanical properties, Materials Science and Engineering A 841 (2022) 143015. https://doi.org/10.1016/j.msea.2022.143015

[23] L. Tan, J. T. Busby, P. J. Maziasz, Y. Yamamoto, Effect of thermomechanical treatment on 9Cr ferritic-martensitic steels, Journal of Nuclear Materials 441 (2013) 713–717. https://doi.org/10.1016/j.jnucmat.2013.01.323

[24] Z. B. Zhang, O. V. Mishin, N. R. Tao, W. Pantleon, Microstructure and annealing behavior of a modified 9Cr-1Mo steel after dynamic plastic deformation to different strains, Journal of Nuclear Materials 458 (2015) 64–69. https://doi.org/10.1016/j.jnucmat.2014.12.001

[25] C. Wei, Z. J. Wang, J. G. Chen, Sulfuration corrosion failure analysis of Inconel 600 alloy heater sleeve in high-temperature flue gas, Engineering Failure Analysis 135 (2022) 106111. https://doi.org/10.1016/j.engfailanal.2022.106111

[26] X. Y. Huang, H. Wang, J. G. Chen, L. H. Dang, Z. Q. Ma, S. B. Cui, Effects of austenitizing temperature on microstructure evolution and corrosion resistance of high Cr ferritic/martensitic steel, International Journal of Electrochemical Science 17 (2022) 220833. https://doi.org/10.20964/2022.08.24

[27] J. G. Chen, C. X. Liu, C. Wei, Y. C. Liu, H. J. Li, Study on microstructure and mechanical properties of direct diffusion bonded low-carbon RAFM steels, Journal of Manufacturing Processes 43 (2019) 192–199. https://doi.org/10.1016/j.jmapro.2019.05.020

[28] X. Wang, J. G. Chen, Y. Guo, W. F. Niu, Effects of heating rate on austenitic transformation and corrosion property of high chromium ferritic/martensitic steel, International Journal of Electrochemical Science 17 (2022) 220818. https://doi.org/10.20964/2022.08.16

[29] C. Wei, Z. J. Wang, X. Wang, Y. Guo, J. G. Chen, Fabrication and assessment of China low activation martensitic (CLAM) steels solid diffusion bonded joint, Fusion Engineering and Design 174 (2022) 112987. https://doi.org/10.1016/j.fusengdes.2021.112987

[30] C. X. Liu, Q. H. Zhao, Y. C. Liu, C. Wei, H. J. Li, Microstructural evolution of high Cr ferrite/martensite steel after deformation in metastable austenite zone, Fusion Engineering and Design 125 (2017) 367–371. https://doi.org/10.1016/j.fusengdes.2017.03.094

[31] C. L. Mao, C. X. Liu, G. W. Liu, L. M. Yu, H. J. Li, J. Dong, Y. C. Liu, The correlation between the microstructural parameters and mechanical properties of reduced activation ferritic-martensitic (RAFM) steel: Influence of roll deformation and medium temperature tempering, Metallurgical and Materials Transactions A 52 (2021) 119–128. https://doi.org/10.1007/s11661-020-06089-1

[32] X. Hu, L. X. Huang, W. Yan, W. Wang, W. Sha, Y. Y. Shan, K. Yang, Evolution of microstructure and changes of mechanical properties of CLAM steel after long-term aging, Materials Science and Engineering A 586 (2013) 253–258. https://doi.org/10.1016/j.msea.2013.08.025

[33] F. Abe, S. Nakazawa, H. Araki, T. Noda, The role of microstructural instability on creep behavior of a martensitic 9Cr-2W steel, Metallurgical Transactions A 23 (1992) 469–477. https://doi.org/10.1007/BF02801164

[34] C. Wei, Y. S. Wei, Z. J. Wang, J. G. Chen, Improving resistance to crack and corrosion of laser-cladded TiC/Co-based composite coatings by doping minor CeO_2, International Journal of Electrochemical Science 17 (2022) 220622. https://doi.org/10.20964/2022.06.02

[35] D. Song, J. Hao, F. Yang, H. Chen, N. Liang, Y. Wu, J. Zhang, H. Ma, E. E. Klu, B. Gao, Y. Qiao, J. Sun, J. Jiang, Corrosion behavior and mechanism of Cr-Mo alloyed steel: Role of ferrite/bainite duplex microstructure, Journal of Alloys and Compounds 809 (2019) 151787. https://doi.org/10.1016/j.jallcom.2019.151787

[36] J. G. Chen, Y. M. Yang, L. Q. Li, Z. J. Wang, H. Y. Xiao, Y. S. Wei, T. H. Zhu, H. Song, Effects of Ti on microstructure, mechanical properties and corrosion behavior of high-strength steel weld metals for offshore structures, International Journal of Electrochemical Science 16 (2021) 210825. https://doi.org/10.20964/2021.08.36

[37] H. Wan, Y. Cai, D. Song, C. Chen, Effect of Cr/Mo carbides on corrosion behaviour of Fe_Mn_C twinning induced plasticity steel, Corrosion Science 167 (2020)

108518.
https://doi.org/10.1016/j.corsci.2020.108518
[38] R. Yuan, X. Yu, Y. Zhang, H. Wu, H. Guo, Research on corrosion mechanism of microstructure on low alloy steel in humid atmosphere, Materials Today Communications 31 (2022) 103715.
https://doi.org/10.1016/j.mtcomm.2022.103715
[39] S. Zhang, H. Li, Z. Jiang, B. Zhang, Z. Li, J. Wu, S. Fan, H. Feng, H. Zhu, Effects of Cr and Mo on precipitation behavior and associated intergranular corrosion susceptibility of superaustenitic stainless steel S32654, Materials Characterization 152 (2019) 141–150. https://doi.org/10.1016/j.matchar.2019.04.010
[40] X. L. Li, L. T. Chang, C. P. Liu, B. Leng, X. X. Ye, F. F. Han, X. M. Yang, Effect of thermal aging on corrosion behavior of type 316H stainless steel in molten chloride salt, Corrosion Science 191 (2021) 109784. https://doi.org/10.1016/j.corsci.2021.109784
[41] T. Y. Sun, Y. J. Guo, Y. M. Jiang, J. Li, Effect of short-time aging on the pitting corrosion behavior of a novel lean duplex stainless steel 2002, Acta Metallurgica Sinica (English Letters) 32 (2019) 755–763. https://doi.org/10.1007/s40195-018-0829-y
[42] S. Y. Lu, K. F. Yao, Y. B. Chen, M. H. Wang, Y. Shao, X. Y. Ge, Effects of austenitizing temperature on the microstructure and electrochemical behavior of a martensitic stainless steel, Journal of Applied Electrochemistry 45 (2015) 375–383. https://doi.org/10.1007/s10800-015-0796-1
[43] H. B. Liu, W. C. Jiao, H. Feng, Z. H. Jiang, C. D. Ren, Influence of austenitizing temperature on the microstructure and corrosion resistance of 55Cr18Mo1VN high-nitrogen plastic mould steel, Acta Metallurgica Sinica (English Letters) 29 (2016) 1148–1160. https://doi.org/10.1007/s40195-016-0506-y
[44] H. Y. Li, C. F. Dong, K. Xiao, X. G. Li, P. Zhong, Relationship between microstructure and corrosion behavior of Cr12Ni3Co12Mo4W ultra-high-strength martensitic stainless steel, Acta Metallurgica Sinica (English Letters) 29 (2016) 1064–1072. https://doi.org/10.1007/s40195-016-0481-3